4. (a) A. D. Johnson, D. G. Coronell, M. S. K. Chen, D. A. Zatko, and J. V. Martinez de Pinillos, in *Contamination Control and Defect Reduction in Semiconductor Manufacturing III,* D. N. Schmidt, Editor, PV 94-9, p. 406, The Electrochemical Society, Pennington, NJ (1994); (b) D. G. Coronell, A. D. Johnson, M. S. K. Chen, S. N. Ketkar, D. A. Zatko, and J. V. Martinez de Pinillos, in *Proceeding of the Institute of Environmental Sciences,* p. 237, Institute of Environmental Sciences, Mount Prospect, IL (1994).
5. G. H. Smudde, M. A. George, J. G. Langan, and W. I. Bailey, in *Microcontamination '92 Conference Proceedings,* p. 487, Canon Communications, Santa Monica, CA (1992).
6. T. A. Tabler, T. G. Wear, and W. Plante, in *Microcontamination '93 Conference Proceedings,* p. 422, Canon Communications, Santa Monica, CA (1993).
7. E. Ozawa, A. Boireau, H. Takagi, M. Miyazaki, H. Chevrel, T. Hattori, and J. Friedt, in *21st Symposium on ULSI Ultra Clean Technology Conference Proceedings,* p. 167, Tokyo, Japan (1994).
8. S. Takahashi, S. Miyoshi, T. Kojima, T. Koyama, and T. Ohmi, in *Microcontamination '93 Conference Proceedings,* p. 596, Canon Communications, Santa Monica, CA (1993).
9. P. W. Atkins, *Physical Chemistry,* p. 1065, W. H. Freeman and Co., San Francisco (1982).
10. (a) S. Miyoshi, T. Lojima, T. Suenaga, T. Ohmi, and Y. Mizuguchi, in *Microcontamination '93 Conference Proceedings,* p. 606, Canon Communications, Santa Monica, CA (1993); (b) J. M. Friedt, H. Chevrel, T. Hattori, H. Takagi, A. Boireau, and E. Ozawa, in *Contamination Control and Defect Reduction in Semiconductor Manufacturing III,* D. N. Schmidt, Editor, PV 94-9, p. 379, The Electrochemical Society, Pennington, NJ (1994).
11. R. Wilson and J. Irven, Personal communication.
12. R. M. Rynders and A. G. Gilicinski, Manuscript in preparation.
13. Matheson Gas Products, *SEMI Tech Brief* (10/93).
14. H. Engels, *Phase Equilibria and Phase Diagrams of Electrolytes,* Chemistry Data Series, Vol. 9, Part 1, p. 102 (1990).

Comparison of AlGaInP Light-Emitting Diodes on n- and p-GaAs Misoriented Substrates Prepared by Low-Pressure Metallorganic Vapor-Phase Epitaxy

Jyh-Feng Lin and Meng-Chyi Wu

Research Institute of Electrical Engineering, National Tsing Hua University, Hsinchu, Taiwan 30043

Ming-Jiunn Jou, Chuan-Ming Chang, and Biing-Jye Lee

Opto-Electronics and Systems Laboratories, Industrial Technology Research Institute, Chutung, Hsinchu, Taiwain 31015

ABSTRACT

The growth and characterization of AlGaInP double-heterostructure orange light-emitting diodes (LEDs) grown on n- and p-GaAs misoriented substrates by low-pressure metallorganic vapor-phase epitaxy are presented. Zinc and silicon are used as p- and n-type dopants for AlGaInP, respectively. The device performance is found to be strongly dependent on the doping concentration in both upper and lower cladding layers for the p-substrate LEDs. However, for the n-substrate LEDs, the strong dependence is only found on the doping concentration in the upper cladding layer. The degradation of device performance with increasing doping concentration in the cladding layer is thought to be due to the light absorption by deep levels. After optimizing the doping concentration in the LEDs, better LED performance can be obtained by using the p-type substrate. This demonstrates the feasibility of fabricating AlGaInP LEDs grown on p-GaAs substrates.

Introduction

High brightness visible light-emitting diodes (LEDs) are very attractive in outdoor applications such as automobile tail lights, moving message panels, and other applications requiring high flux outputs. Although bright red AlGaAs LEDs have been available for several years, the low brightness of commercial $GaAs_{1-y}P_y$ and GaP LEDs of other colors limits the outdoor display in a broad color application.

Quaternary AlGaInP alloy compounds have been extensively investigated for possible applications in optical devices operating in the visible spectral region. The introduction of AlGaInP LEDs, lattice-matched to GaAs, has spaced the color range from red-orange to green because of the high brightness in these LEDs. [1-4] It has been successful in the fabrication of AlGaInP LEDs for exhibiting an external quantum efficiency of 6%, [1] 1.5% at 620 nm, [3] and 0.7% at 573 nm. [4] In these works, AlGaInP LEDs were usually prepared on the n-GaAs substrates. However, there are no reports on the AlGaInP LEDs grown on p-GaAs substrates. Furthermore, very efficient red AlGaAs LEDs grown on p-GaAs substrates have been reported by Varon *et al.*[5] Interest is thus exhibited in the fabrication of AlGaInP LEDs by using p-type GaAs as a substrate.

In this paper, for the first time, we investigate the doping effects in the upper and lower cladding layers for both n- and p-substrate AlGaInP LEDs. The LEDs were grown on 2, 10, and 15°-off n-type substrates as well as 2 and 15°-off p-type substrates by low-pressure metallorganic vapor-phase epitaxy (LP MOVPE). After optimizing the doping concentrations in both cladding layers, the device performance of the n- and p-substrate LEDs are compared in detail.

Experimental

The epilayers were grown in a LP MOVPE reactor with gas-flow rotating susceptor heated by infrared lamps. The trimethylalkyls of aluminum, gallium, and indium were used as the group III sources. Pure arsine and phosphine were the group V reactants. The p- and n-type doping sources were dimethylzinc (DMZn) and disilane (Si_2H_6), respectively. The misoriented substrates were tilted off (100) plane toward [011] direction by angles of 2, 10, and 15°. The LED structure, as shown in Fig. 1, consists of a 0.5 μm GaAs buffer layer, a 0.5 μm $(Al_{0.7}Ga_{0.3})_{0.5}In_{0.5}P$ lower clad-

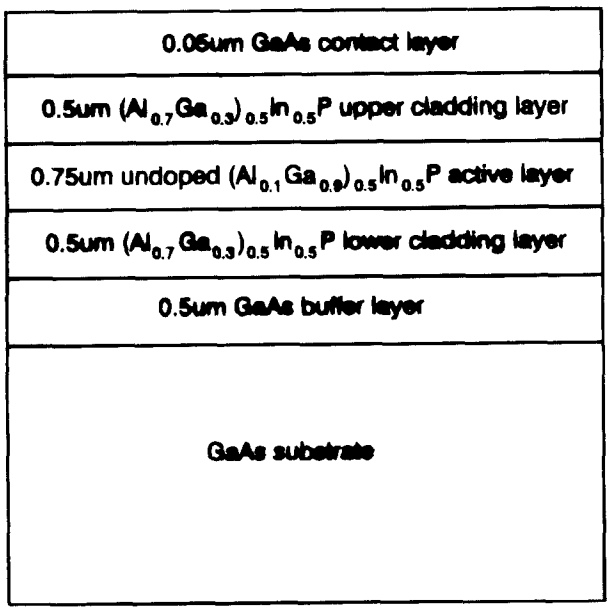

Fig. 1. Schematic structure of AlGaInP DH LEDs.

ding layer, a 0.75 μm undoped $(Al_{0.1}Ga_{0.9})_{0.5}In_{0.5}P$ active layer, a 0.5 μm $(Al_{0.7}Ga_{0.3})_{0.5}In_{0.5}P$ upper cladding layer, and a 0.5 μm GaAs contact layer. The DH layers were grown at a growth temperature of 760°C and a V/III ratio of 200. The degree of lattice mismatch between the epilayer and the substrate, determined by double-crystal x-ray diffraction, is generally less than 0.1%. The photoluminescence (PL) was excited by using the Ar^+ laser 488 nm line, and the PL signal was detected with a silicon p-i-n detector.

The p and n ohmic contacts of the LEDs were Au/AuZn and Au/Ni/AuGe, respectively. The wafer was annealed at 500°C for 5 min in the N_2 ambient. The top ohmic contact and GaAs cap layer outside the upper AlGaInP cladding layer were again chemically etched away in sequence using a 10 g KI:1 g I_2:100 cm^3 H_2O and a $5H_2SO_4$:$1H_2O_2$:$1H_2O$ solution, respectively, through defined pattern by photolithography to allow light emission through the top of the die. The wafer was then sawn into individual chips of 300 × 300 μm. The chip was attached and bonded to a TO-5 package. Electroluminescence (EL) was used to characterize the emission spectra of LEDs. Light output measurements were made by using an integrating sphere and detector with calibrations traceable to the National Institute of Standards and Technology.

Results and Discussion

The luminous efficiency of LEDs relates strongly to the doping characteristics and other parameters such as injection efficiency, doping levels and activation of dopants, junction placement, degree of diffusion of dopants, spreading of injection currents, interfacial recombination, and light absorption by defects or deep levels. In this study, a simple double heterostructure is grown on both n- and p-type misoriented substrates under the same growth conditions with the only difference in the growth sequence. For the n-substrate LEDs, the undoped $(Al_{0.1}Ga_{0.9})_{0.5}In_{0.5}P$ active layer is sandwiched by the p-type $(Al_{0.7}Ga_{0.3})_{0.5}In_{0.5}P$ upper cladding layer and the n-type $(Al_{0.7}Ga_{0.3})_{0.5}In_{0.5}P$ lower cladding layer. The same undoped active layer in the p-substrate LEDs is sandwiched by the n-type upper cladding layer and the p-type lower cladding layer.

Figures 2a and b show the luminous intensity as a function of the [DMZn] in the upper cladding layer for the n-substrate LEDs and in the lower cladding layer for the p-substrate AlGaInP LEDs, respectively. The luminous intensity is first increased and then decreased as [DMZn] increases. For both n- and p-substrate LEDs with the same 15°-off misoriented angle, the maximum luminous intensity is achieved with the [DMZn] in the range of 1.33×10^{-5} to 7×10^{-6} and 1.33×10^{-5} to 2.66×10^{-5}, respectively. In the lower range of [DMZn], the low luminous intensity is due to the insufficiency of carrier injection. The hole concentration and the electrical activity of Zn is increased with increasing substrate tilt angle due to the increased [01$\bar{1}$] step density on the substrate surface, together with an increase in the tilt angle toward the [011] direction.[6-9] This behavior leads to a strong dependence of luminous intensity on the misoriented angle of substrates. The fact that the maximum luminous intensity of the LEDs with a smaller misoriented angle is lower than that of the LEDs with a larger misoriented angle is attributed to the lower electrical activity of Zn in the AlGaInP LEDs with a lower misoriented angle. In the higher [DMZn] range, a further increase of the [DMZn] will result in a decrease in the luminous intensity. For a surface emission structure, this fast decrease of luminous intensity can be ascribed to the increase of light absorption by the upper cladding layer. Nozaki and Ohba[10] found that the Zn-doped AlGaInP layers exhibit a deep level originating from the Zn-related defects, and the deep-level concentration is proportional to the Zn concentration. The deep levels, which will increase with [DMZn], in the upper cladding layer cause a light absorption from the active layer, and thus degrades the luminous intensity. On the other hand, the stronger dependence of the luminous intensity on the [DMZn] is obtained from the n-substrate LEDs. The less dependence of the luminous intensity on the misoriented angle of the p-substrate LEDs as compared to that of the n-substrate LEDs shows another evidence for the explanation of light absorption by the Zn-related deep levels. On the other hand, as the [DMZn] is high, the decrease of luminous in-

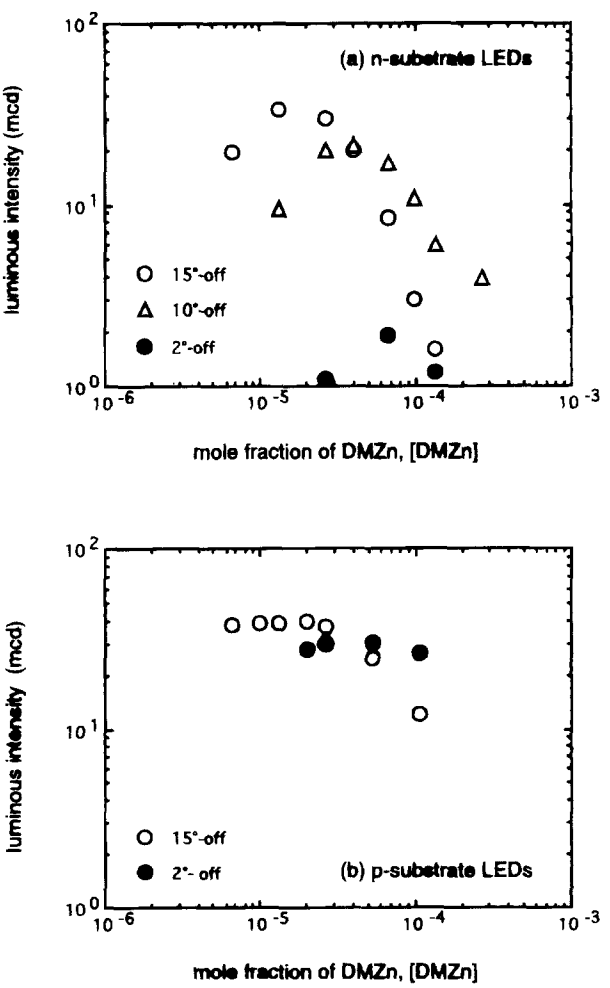

Fig. 2. The dependence of the luminous intensity as a function of the [DMZn] (a) in the upper cladding layer for the n-substrate LEDs, and (b) in the lower cladding layer for the p-substrate AlGaInP LEDs.

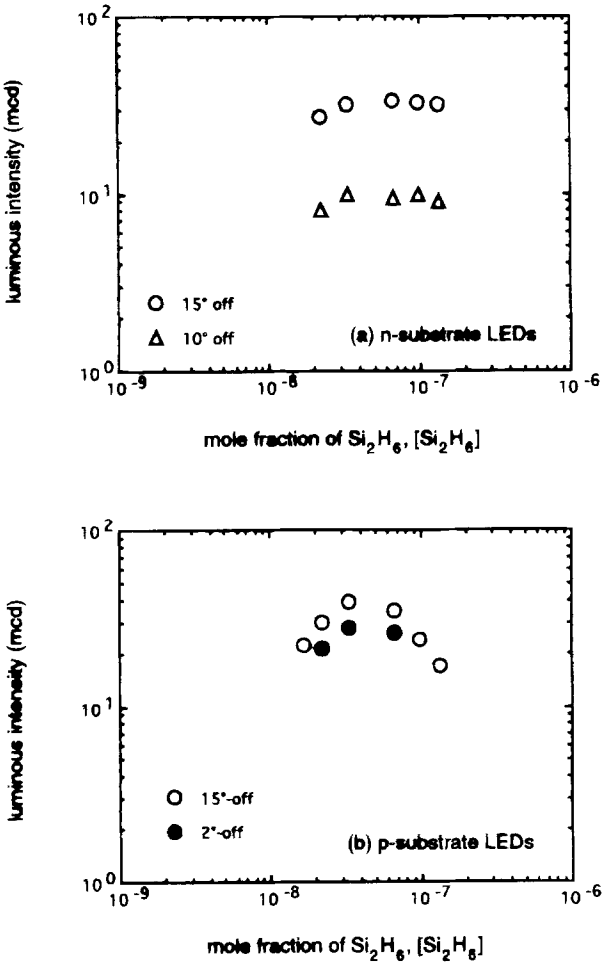

Fig. 3. The dependence of luminous intensity as a function of the [Si_2H_6] (a) in the lower cladding layer for the n-substrate LEDs, and (b) in the upper cladding layer for the p-substrate LEDs.

tensity for the p-substrate LEDs as the increase of the [DMZn] is mainly caused by the increase of the interfacial recombination. For the 2°-off p-substrate LEDs, the slower decrease of the luminous intensity as the increase of the [DMZn] than that of 15°-off p-substrate LEDs is due to the less incorporation of Zn. The maximum luminous intensity of the 2°-off p-substrate LEDs is lower than that of 15°-off p-substrate LEDs. This is because the electrical activity of Zn in the 2°-off p-type AlGaInP is lower than that in the 15°-off AlGaInP.

Similarly, the effects of Si-doped characteristics on LED performance are investigated by the different misoriented substrates. Figures 3a and b show the luminous intensity as a function of the [Si_2H_6] in the lower cladding layer for the n-substrate LEDs and in the upper cladding layer for the p-substrate LEDs, respectively. The [DMZn] in the cladding layers for both n- and p-substrate LEDs was kept constant at 1.3×10^{-5}, which is the optimum doping level for 15°-off LEDs. For the n-substrate LEDs, the luminous intensity is less dependent on the [Si_2H_6] in the range studied, except for the insufficiency of carrier injection in the low [Si_2H_6]. The decrease of the luminous intensity as the increase of the mole fraction of dopant in the lower cladding layer, which was observed from the p-substrate LEDs, was not obtained from the n-substrate LEDs in this doping range. This is because the low [Si_2H_6] was used in this study due to the higher doping efficiency of Si in AlGaInP than that of Zn. As the [Si_2H_6] increases, there is a similar tendency of the luminous intensity for both 10° and 15°-off n-substrate LEDs because the incorporation and the electrical activity of Si are less dependent on the misoriented angle.[10] As shown in Fig. 3b, the luminous intensity decreases with increasing [Si_2H_6] for the p-substrate LEDs. This is due to the optical absorption by deep levels introduced at higher doping levels in the AlGaInP layer, as reported by Suzuki *et al.*[11] and Nojima *et al.*[12] For the p-substrate LEDs, the luminous intensity is strongly dependent on the mole fraction of dopant in the upper cladding layer, as observed from the p-substrate LEDs. However, the less misorientation dependence of Si-doped efficiency in AlGaInP makes the luminous intensity of the p-substrate LEDs less dependent on the misoriented angle than that of the n-substrate LEDs.

As observed in Fig. 3, the luminous intensity is strongly dependent on the misorientation angle of the GaAs substrate. With increasing tilt angle, the step density on the substrate surface increases or the step interval decreases. When the substrate is tilted toward the [011] direction, the step-edge surface consists of dangling bonds from the group III atoms. Under the group V stabilized condition, the adsorption of a group V atom on a single dangling bond will take place with a higher probability.[13] Together with two dangling bonds from the terrace and one dangling bond from the step edge, a stable adsorption site for the group III atom is formed when the substrate is tilted toward the [011] direction. Thus, an enhancement in the step and two-dimensional growth and a stronger luminous intensity with increasing tilt angle will result.[14]

Figure 4 shows the 300 K EL spectra at 20 mA for n- and p-substrate LEDs with different misoriented angles. The longer peak wavelength from the LEDs with smaller tilted angle is mainly caused by the Cu-Pt-type ordering structure.[15,16] The peak wavelength is effectively shortened from

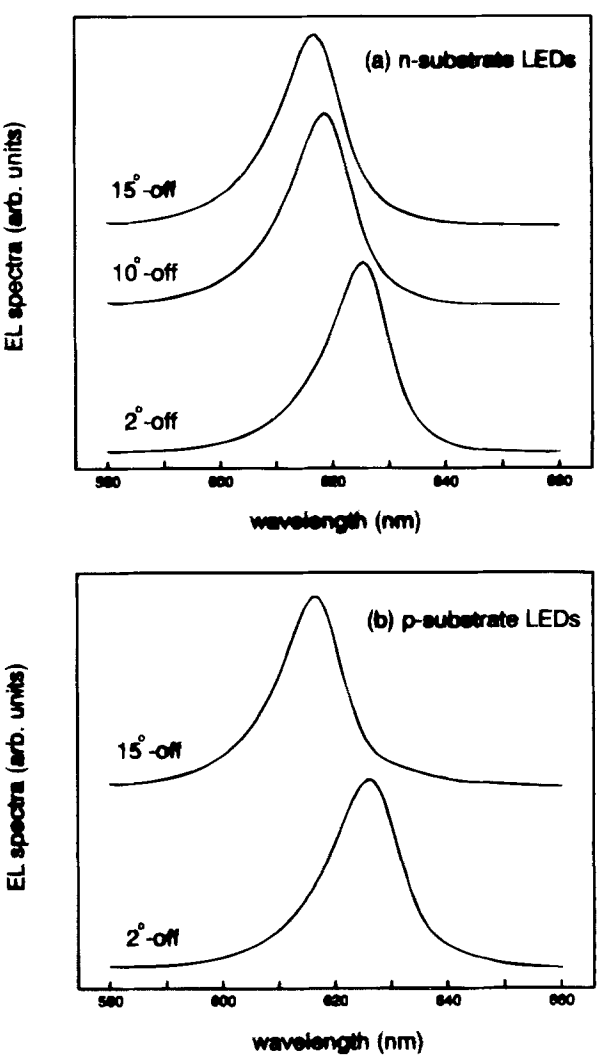

Fig. 4. 300 K EL spectra measured from (a), 2, 10, and 15°-off n-substrate LEDs, and (b) 2 and 15°-off p-substrate LEDs.

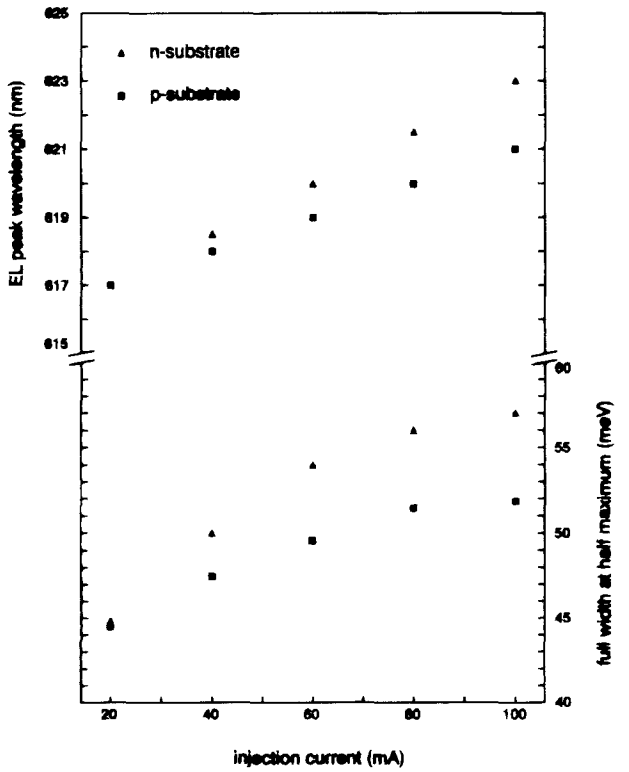

Fig. 5. (a) 300 K EL peak wavelength and (b) full width at half maximum operating at different injection currents obtained from 15°-off n- and p-substrate LEDs.

626 nm for the 2°-off LEDs to 617 nm for the 15°-off LEDs. The spectra shapes obtained from n- and p-substrate LEDs are almost the same.

The peak wavelength and full width at half maximum (FWHM) of EL spectra obtained by operating the LEDs under different injection currents are shown in Fig. 5. The degradation of device performance for the n-substrate LEDs, including the increase in peak wavelength and FWHM of the EL spectra due to joule heating, is more significant than that for the p-substrate LEDs. It is attributed to the higher series resistance of p-type upper cladding layer in the n-substrate LEDs than that of n-type upper cladding in the p-substrate LEDs.

Figure 6 shows the light output power *vs.* the dc current from the n- and p- substrate LEDs. The output power increases with increasing the injection current, saturates at around 80 mA, and decays at high currents. Joule heating and carrier leakage from the active region are possible causes for this output power saturation.[17,18] The light output powers of 200 and 240 μW at 20 mA correspond to the external quantum efficiency of 0.5 and 0. 6% for the n- and p-substrate LEDs, respectively. The higher output power obtained from the p-substrate LEDs than that from the n-substrate LEDs may be attributed to the less dopant-related deep levels, the better current spreading, or the higher mobility in the n-type upper cladding layers of the p-substrate LEDs.

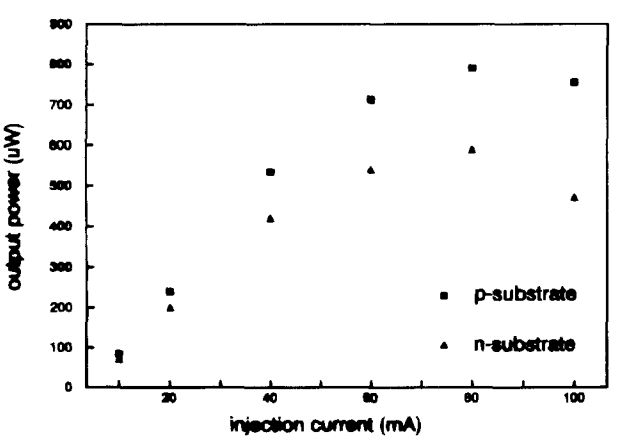

Fig. 6. The output power of bare chips operating at different injection currents obtained from 15°-off n- and p-substrate LEDs.

As observed in Fig. 2a and 3b, the luminous intensity is sensitive to the doping level in the upper cladding layer, particularly when it has a conductivity type opposite to that of the substrate. The lower cladding layer has a uniform current injection through the GaAs substrate, whereas the current spreading from the patterned top ohmic contacts and the 0.05 μm GaAs top contact layer plays an important role for the upper cladding layer. It is expected that by the introduction of a thick, high bandgap and low resistance window layer on the upper cladding layer will maximize light extraction and minimize current crowding from the LEDs. GaP [1] and AlGaAs with high Al compositions[3,4] are usually used as the window layer or current spreading layer. We report that the external quantum efficiency of the AlGaInP DH LEDs can be improved to 3.5% by growing a 7.5 μm MOVPE-grown GaP window layer.

Conclusions

We demonstrate the feasibility in the growth and fabrication of DH AlGaInP LEDs on p-GaAs substrates grown by LP MOVPE. The differences in the device performance between the n- and p-substrate LEDs with different misoriented substrates are compared in detail. In this study, the device performance is found to be strongly dependent on the doping concentration in the upper and lower cladding layer for the p-substrate LEDs. However, for the n-substrate LEDs, the strong dependence is only found on the doping concentration in the upper cladding layer. Furthermore, the difference of maximum light output between 2°- and 15°-off p-substrate LEDs is less than that of n-substrate LEDs. This suggests that it may be not necessary to use misoriented substrates if p-GaAs wafer is utilized as the substrate of AlGaInP LEDs.

Acknowledgments

The authors gratefully acknowledge the Ministry of Economic Affairs, Republic of China, under Project Number 3AA1100. The financial support from the National Science Council is also appreciated (NSC 83-0417-E-007-009).

Manuscript submitted July 8, 1994; revised manuscript received Dec. 16, 1994.

National Tsing Hua University assisted in meeting the publication costs of this article.

REFERENCES

1. K. H. Huang, J. G. Yu, C. P. Kuo, R. M. Fletcher, T. D. Osentowski, L. J. Stinson, M. G. Craford, and A. S. H. Liao, *Apply. Phys. Lett.*, **61**, 1045 (1992).
2. R. M. Fletcher, C. P. Kuo, T. D. Osentowski, K. H. Huang, M. G. Craford, and V. M. Robbins, *J. Electron. Mater.*, **20**, 1125 (1991).
3. H. Sugawara, M. Ishikawa, and G. Hatakoshi, *Appl. Phys. Lett.*, **58**, 1010 (1991).
4. H. Sugawara, K. Itaya, H. Nozaki, and G. Hatakoshi, *ibid.*, **61**, 1775 (1992).
5. J. Varon, M. Mahieu, P. Vandenburg, M. Boissy, and J. Lebailly, *IEEE Trans. Electron. Devices*, **ED-28**, 416 (1981).
6. J. F. Lin, M. C. Wu, M. J. Jou, C. M. Chang, and B. J. Lee, *Jpn. J. Appl. Phys.*, **33**, L857 (1994).
7. H. Hamada, M. Shono, S. Honda, R. Hiroyama, K. Yodoshi, and T. Yamaguchi, *IEEE J. Quantum Electron.*, **QE-27**, 1483 (1991).
8. M. Suzuki, Y. Nishikawa, M. Ishikawa, and Y. Kokubun, *J. Cryst. Growth*, **113**, 127 (1991).
9. J. F. Lin, M. J. Jou, C. Y. Chen, and B. J. Lee, *ibid.*, **124**, 415 (1992).
10. C. Nozaki and Y. Ohba, *J. Appl. Phys.*, **66**, 5394 (1989).
11. M. Suzuki, M. Ishikawa, K. Itaya, Y. Nishikawa, G. Hatakoshi, and Y. Kokubun, *J. Cryst. Growth*, **115**, 498 (1991).

12. S. Nojima, H. Tanaka, and H. Asahi, *J. Appl. Phys.*, **59**, 3489 (1986).
13. M. Kondo, C. Anayama, T. Tanahashi, and S. Yamazaki, *J. Cryst. Growth*, **124**, 449 (1992).
14. J. F. Lin, M. C. Wu, M. J. Jou, C. M. Chang, and B. J. Lee, *ibid.*, **142**, 15 (1994).
15. A. Gomyo, T. Suzuki, K. Kobayashi, S. Kawata, I. Hino, and T. Yuasa, *Appl. Phys. Lett.*, **50**, 673 (1987).
16. Y. Ohba, M. Ishikawa, H. Sugawara, M. Yamamoto, and T. Nakanishi, *J. Crystal Growth*, **77**, 374 (1986).
17. R. C. Goodfellow, A. C. Carter, G. J. Rees, and R. Davis, *IEEE Trans. Electron Devices*, **ED-28**, 365 (1981).
18. S. Yamakoshi, O. Hasegawa, H. Hamaguchi, M. Abe, and T. Yamaoka, *Appl. Phys. Lett.*, **31**, 627 (1977).

The Effects of HF Cleaning Prior to Silicon Wafer Bonding

Karin Ljungberg, Ylva Bäcklund,* and Anders Söderbärg

Department of Technology, Uppsala University, S-751 21 Uppsala, Sweden

Mats Bergh, Mats O. Andersson, and Stefan Bengtsson*

Department of Solid State Electronics, Chalmers University of Technology, S-412 96 Göteborg, Sweden

ABSTRACT

The effects of preparation of silicon surfaces in hydrofluoric acid (HF) solutions, prior to direct wafer bonding, is investigated. Surface analysis with atomic force microscopy, electron spectroscopy for chemical analysis, and estimation of the surface particle density is made. This is related to results from room temperature bonding experiments. A diluted (1-10%) HF solution is most favorable for hydrophobic silicon wafer bonding. The subsequent water rinse should be omitted, or performed in a careful way, to avoid particle contamination. HF:NH_4F solutions generally are not favorable for bonding. The initial room temperature bonding is attributed to the relatively weak van der Waals forces, which makes the bonding sensitive to the surface roughness and particle density. The surface chemistry appears to have a second order influence in hydrophobic bonding.

Introduction

Since the first report on silicon wafer bonding by Lasky and co-workers in 1985,[1] most bonding work published has dealt with hydrophilic surfaces, *i.e.*, the wafers are covered by a thin chemically grown oxide. It has been reported that hydrophilic surfaces are necessary for initial spontaneous bonding to occur, and that hydrophobic surfaces can be bonded only with the aid of an applied pressure.[2] In contrast, we have shown that spontaneous bonding also occurs for hydrophobic oxide-free surfaces.[3,4] Bonding of silicon wafers without any interfacial oxide is important, *e.g.*, for high power devices and as an alternative to epitaxial layers. Hydrophilic bonding always gives an interfacial oxide, resulting in an unacceptably high density of electron states at the interface.[5]

Since there are different opinions regarding the possibility of achieving spontaneous hydrophobic bonding, a closer investigation of how different cleaning processes affect the surfaces is essential. The initial room temperature bonding of hydrophobic surfaces has been attributed to van der Waals forces.[3,6] However, there are other authors arguing that the hydrophobic surface attraction is due to hydrogen bonds between fluorine or hydroxyl (OH) groups, coupled to the surface dangling bonds.[7,8] This should be compared to the initial bonding between hydrophilic surfaces, which has been attributed to hydrogen bonds between OH groups on the surfaces.[1,9]

Van der Waals interactions result from the charge distribution variations, causing temporary dipole moment in the molecules.[10] The forces are weak (5-20 kJ/mol) and the attraction energy decreases with the sixth power of the distance.[11] In case van der Waals forces are causing the attraction, the bonding process is very sensitive to the surface morphology. A somewhat stronger interaction is caused by so-called hydrogen bonds. These are formed when a hydrogen atom attracts two highly electronegative atoms, particularly N, O, and F, and the energies in this case reach values of 20-30 kJ/mol. If such bondings can be achieved between two mating surfaces, the initial, room temperature, bonding is stronger.

It has been observed that a water rinse after the HF etch has a negative effect on the room temperature bondability,[4] but the cause is still unclear. Different contact wave velocities for different concentrations of the HF etchant also were observed. The contact wave is observed as the movement of the border of the bonded area. It is observed by use of infrared light to which the silicon wafer is transparent. In this work we further investigate the effects on surface morphology, chemistry, and bondability after various pretreatments. We have cleaned silicon wafers in various HF solutions and characterized the cleaned surfaces with regard to surface roughness, chemical nature, and particle density. The roughness was measured with an atomic force microscope (AFM) and the chemical nature was measured using electron spectroscopy for chemical analysis (ESCA). The particle density was estimated using dark field microscopy. The results are then compared to results from bonding experiments.

Experimental

Room temperature bonding.—The silicon wafers used were 3 in. [100]- and [111]-oriented wafers, with a thickness of 380 ± 5 μm (Wacker, FZ, 10-12 Ω cm, n- and p-doped). All experiments were performed in a clean room environment. The wafers were etched for 1 to 10 min in aqueous HF solutions (aqHF), with concentrations between 1 and 50%, or buffered HF solutions (BHF), *i.e.*, HF(50%):NH_4F(40%) 1:7 or 1:20. All wafers were blown dry in N_2 after etching. When the wafers are contacted, the contact area spreads like a wave over the whole wafer. This wave was observed in transmitted infrared (IR) light, using an IR camera and a video setup. Normally, a slight pressure with the tweezers at the wafer edge was required to initiate the wave. If the contact area then grows without further help, the bonding is referred to as spontaneous.

AFM.—An atomic force microscope was used to characterize the silicon surfaces regarding topography and roughness. The AFM (Park Scientific Instruments Model SFM-BD2-210) operates at room temperature, under a flow of dry nitrogen gas. The instrument was used in the contacting mode, wherein the sample acts to deflect the Si_3N_4 tip and cantilever by a repulsive force. The topography of the sample is represented by the piezo driving voltage required to keep this deflection constant. The image processing be-

* Electrochemical Society Active Member.